https://doi.org/10.1007/s41230-026-4216-4

Position-dependent microstructural characteristics of gravity casting TiAl turbocharger turbine

Han Liu[1, 2, 3], *Zhi-jun Ji[1, 2, 3], Ye Liu[4], Xian-fei Ding[1, 2, 3], and Hai Nan[1, 2, 3]

1. AECC Beijing Institute of Aeronautical Materials, Beijing 100095, China

2. BAIMTEC Material Co., Ltd., Beijing 100094, China

3. Beijing Engineering Research Center of Advanced Titanium Alloy Precision Forming Technology, Beijing 100095, China

4. China North Engine Research Institute, Tianjin 300400, China

Abstract: To reveal the microstructural characteristics at specific locations of a TiAl turbocharger turbine under gravity casting conditions, metallographic observations were conducted on characteristic regions of its longitudinal section. The turbine hub exhibits primarily a columnar microstructure, with an average grain size significantly larger than that of the blade, which exhibits an equiaxed microstructure. The cooling rate varies significantly across the turbine, decreasing from the blade tip to the hub bottom, resulting in a negative correlation with grain size. The center of the turbine hub and the blade tips show higher γ phase volume fractions (14.028% and 10.009%, respectively). In terms of phase constitution, both a low Ti/Al atomic ratio and a high cooling rate shift the solidification path to the Al side of the phase diagram, promoting the precipitation of massive γ phase. The average hardness of the blade body (273.89 HV) is higher than that of the turbine hub (238.40 HV), while the blade root (282.66 HV) exhibits similar average hardness to the blade body.

Keywords: TiAl turbocharger turbine; gravity casting; microstructural characteristics; phase constitution; solidification path

CLC numbers: TG146.23 **Document code:** A **Article ID:** 1672-6421(2026)04-515-08

1 Introduction

TiAl alloys are characterized by high specific strength, outstanding oxidation resistance, and excellent mechanical properties at elevated temperatures, which have great potential for high-temperature applications in aerospace and automotive fields[1-5]. Typically, the service temperature of the exhaust valves and turbocharger turbines is in the range of 750–950 °C[6]. Replacing traditional Ni-based superalloys with TiAl alloys can effectively reduce structural weight and improve engine acceleration responsiveness[7-9]. For instance, TiAl turbines can exhibit 0.2 s improvement in time to achieve the required supercharging pressure[10]. Furthermore, Zhu et al.[11-13] conducted extensive work on the composition, microstructure, and mechanical properties of centrifugally casting turbines with a nominal composition of Ti-47.5Al-2.5V-1Cr-0.2Zr, which possesses both high mechanical properties and good casting processability. Consequently, this alloy composition was selected for the turbine investigated in the present work.

Numerical simulation can model the flow behavior of molten metal during mold filling and the thermal distribution during solidification, thereby predicting microstructural characteristics. Sung et al.[14] conducted modeling analysis on TiAl alloy turbine casting and found that the melt fluidity approximately linearly increased with mold preheating temperature under centrifugal conditions. Hu et al.[15] obtained a near-complete turbine using the centrifugal top injection method, based on the casting parameters obtained by numerical simulation. Zhao et al.[16] optimized the mold preheating temperatures and centrifugal rotational rates of the turbine mold based on numerical simulations, eliminating misrun and gas porosity defects. However, the variation of the solidification temperature gradient has a decisive influence on the microstructure of castings. The studies above mainly focused on the

***Zhi-jun Ji**

Male, born in 1986, Ph. D., Senior Engineer. His research interests mainly focus on titanium alloy and TiAl alloy casting, and the hybrid forming of the casting and the additive manufacturing.

E-mail: jzjbiam@sina.com

Received: 2024-10-29; Revised: 2025-06-16; Accepted: 2025-12-28

optimization of the casting process under centrifugal casting conditions, not targeted at improving microstructure formation through simulation on the temperature field during the filling and solidification process.

Zhu et al.[17] demonstrated that, for thin-walled TiAl alloy castings, gravity casting exhibited much better melt-filling stability and synchronization compared with centrifugal casting. Gravity casting can reduce the turbulent filling and thermal shock caused by the mold rotating process, thereby facilitating the smooth filling of the casting and reducing the defects of mold particle inclusions. Due to the solidification shrinkage compensation of casting processes and geometrical characteristics of molds, the turbocharger turbines exhibited significant differences in microstructure and phase constitution at different positions[18]. Clarifying these variations is essential for the practical application of TiAl turbines.

This work investigated the position-dependent microstructural characteristics of a Ti-47.5Al-2.5V-1Cr-0.2Zr (at.%) turbocharger turbine fabricated by gravity casting. The macrostructure, microstructure, Ti/Al atomic ratio, and microhardness distribution were analyzed across different characteristic locations on the longitudinal section. The results provide insights into microstructural heterogeneity, contributing to the optimization of the gravity casting process for TiAl turbines and promoting the broader engineering application of TiAl turbocharger turbines.

2 Experimental procedures

The nominal composition of the turbocharger turbine in this work was Ti-47.5Al-2.5V-1Cr-0.2Zr (at.%). The turbocharger turbines with a diameter of 125 mm, a height of 66 mm and a minimum section thickness of 1 mm were prepared by gravity investment casting, using a vacuum consumable electrode arc furnace. The Y_2O_3 ceramic oxide mold was used, with a preheating temperature of 800 °C and a pouring temperature of 1,600 °C.

Following the solidification process, hot isostatic pressing (HIP) was conducted at (1,200–1,300) °C/150 MPa for 1 h, and subsequently, vacuum annealing heat treatment (HT) was conducted at 900–1,000 °C for 15 h, according to the parameters proposed by Zhu et al[13]. Specimens for analysis of chemical composition were taken at different positions of the turbine. The actual composition of the specimens was found to be very close to the nominal composition of the alloy, as shown in Table 1.

Subsequently, the turbine was cut along the centerline of the hub to acquire the longitudinal section. The sampling positions of metallographic specimens cover the turbine's hub and blades, as shown in Fig. 1. The specimens were divided into three groups according to sampling positions. Specimens 1 (upper hub), 3 (middle hub), and 5 (lower hub) were located at the turbine's hub, Specimens 2 (leading edge) and 4 (surface of hub) were located at the blade root, and Specimens 6 (upper tip), 7 (center), and 8 (lower tip) were located at the blade body. These specimens can effectively represent the microstructural characteristics of different regions across the entire turbine.

Table 1: Chemical compositions of TiAl turbine (at.%)

Elements	Al	V	Cr	Zr	Ti
Nominal	47.5	2.5	1	0.2	Bal.
Actual	47.37	2.48	0.93	0.19	Bal.

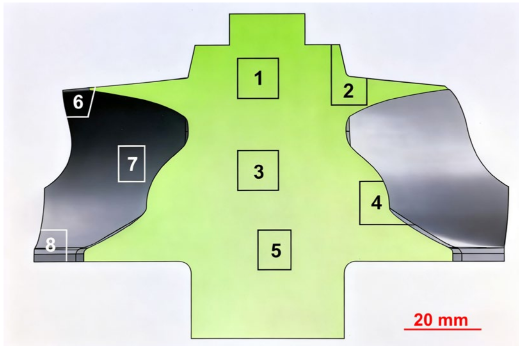

Fig. 1: Sampling positions of metallographic specimens along longitudinal section of a turbine

The metallographic specimens were polished and then corroded in a solution composed of 2%HF+3%HNO_3+95%H_2O (vol.%) for 5 s. Then, the microstructure was observed using a metallographic microscope and a field emission scanning electron microscope (SEM). Chemical composition analysis was performed using an energy dispersive spectrometer (EDS) attached to the microscope. Phase volume fraction was manually counted based on five metallographic images.

It is difficult to undertake tensile tests at various critical locations because of the complex structure of turbine. Therefore, hardness, which correlates positively with strength, is used to reflect the strength characteristics. The grain size evaluation was conducted using the linear intercept method in accordance with GB/T 6394-2017. A load of 50 gf was applied for Vickers-hardness test, five equidistant points were selected on a single metallographic specimen to calculate the average microhardness value. After polishing the longitudinal and cross sections of the turbine, Rockwell hardness tests were conducted.

In order to analyze the microstructural characteristics at different positions, a numerical simulation for pouring and solidifying processes was conducted using ProCAST 2022.

3 Results and discussion

3.1 Microstructure of turbine

The simulation results of the cooling rates along the turbine's longitudinal section are shown in Fig. 2, as the temperature drops from near the liquidus (T_{liq}, 1,492 °C), to the temperature near the solidus (T_{sol}, 1,457 °C). When the turbine cools to below T_{sol}, the distribution of temperature on the longitudinal section is shown in Fig. 3. The simulation results indicate that the cooling rate of the upper hub is higher than that of the

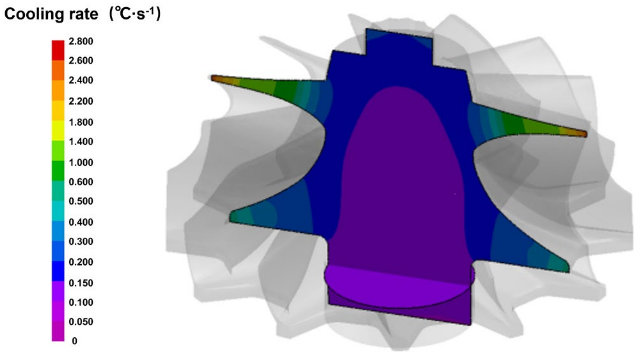

Fig. 2: Cooling rates on longitudinal section of turbine (from 1,492 °C to 1,457 °C)

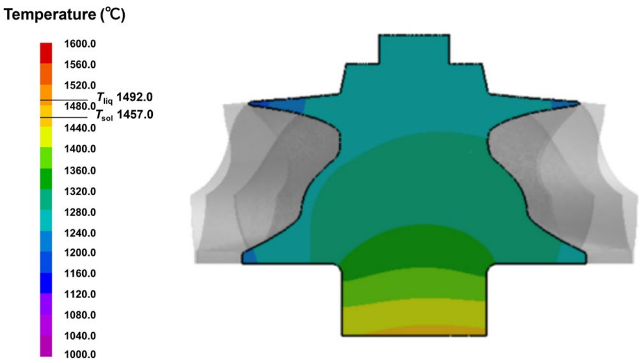

Fig. 3: Temperature field during filling and solidification process of turbine (*t*=391 s)

lower hub, the blade exhibits a higher cooling rate than the hub, and the upper blade tip exhibits the highest cooling rate.

Figure 4 shows the macrostructure of the metallographic specimens. The surface features equiaxed fine grains, from which a number of grains grow inward toward the center of the casting, developing a columnar grain structure. At the turbine hub, as shown in Figs. 4(a), (c) and (e), the top, middle, and bottom positions of the hub exhibit a coarse columnar structure. The growth direction of columnar grains is generally from the edge to the center of the casting, that is, along the opposite direction of the heat flow. At the blade root, as shown in Figs. 4(b) and (d), regions with obvious fine grains are found. At the blade tips, as shown in Figs. 4(f) and (h), a significant number of fine columnar grains are observed, with their growth orientation extending from the edge towards to the center of the specimen. These fine columnar grains are discontinuous. At the center of the blade body, as illustrated in Fig. 4(g), no columnar grains are observed; instead, this region is composed entirely of equiaxed grains. This phenomenon may be associated with the rapid cooling rate and anisotropic heat dissipation subsequent to melt filling.

The hub and blade root regions exhibit relatively larger average grain sizes, while the blade body regions exhibit smaller average grain sizes. The average grain size at different positions of the specimens was calculated, as shown in Table 2. Comparing Table 2 with Fig. 2, there is a clear negative correlation between the average grain size and the cooling rate.

The HIP and HT processes do not affect the morphology of the lamellar grains, but only produce a small amount of massive γ phases, with sizes in tens of micrometers, precipitated at the grain boundary. The precipitated γ has benefit for the strength and plasticity at room temperature, as well as the creep resistance at high temperatures. Metallographic microscope observations show that the microstructure comprises (α_2+γ) lamellar colonies and randomly distributed massive γ phases. The lamellar colonies appear as columnar or equiaxed grains, with lamellae structures within the grain boundaries. The massive γ phases exhibit flat grain boundaries and uniform internal characteristics, appearing light or dark under

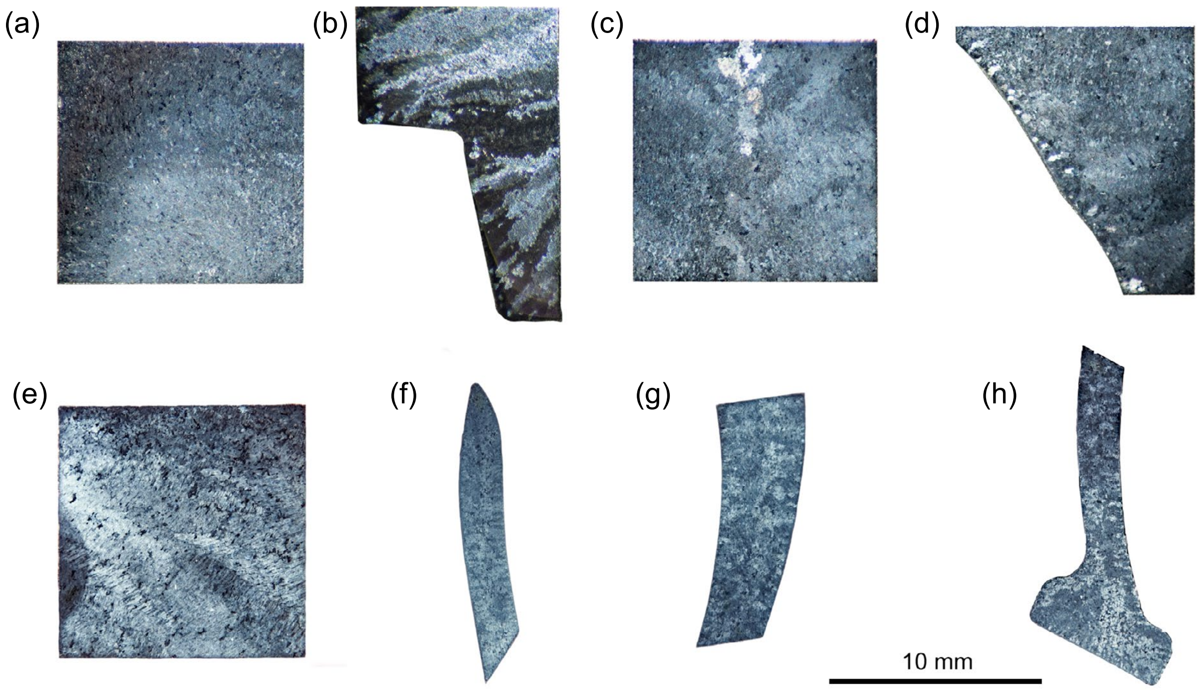

Fig. 4: Macrostructures of metallographic specimens corresponding to Specimens 1–8, respectively (a)–(h)

Table 2: Average grain size of different metallographic specimens

Specimen number	Number of grains per unit area (mm^{-2})	Average grain size (mm^2)
1	35.84	0.0279
2	11.79	0.0848
3	17.44	0.0573
4	18.22	0.0549
5	6.28	0.1592
6	228.77	0.0044
7	48.44	0.0206
8	163.84	0.0061

microscope after etching.

For the specimens at the turbine hub, as shown in Figs. 5(a), (c) and (e), the edge positions are dominated by columnar grains, with some massive γ phases precipitate at the columnar grain boundaries, as pointed out in Fig. 5(a). The volume fraction of massive γ phase at the center is significantly higher than that at the edge, but the structure still mainly consists of columnar grains.

For the metallographic specimens at the blade root (Specimens 2 and 4), a significant difference in microstructure was observed between the region adjacent to the blade body and that adjacent to the turbine hub. As shown in Figs. 6(a) and (c), for the region adjacent to the hub, the columnar grains are coarse and continuous, with a maximum width of 1,000 μm. The region adjacent to the blade body exhibits a higher cooling rate and a higher degree of supercooling, resulting in the formation of columnar grains with widths of 200–400 μm, as shown in Figs. 6(b) and (d). These grains are discontinuous, accompanying with the formation of equiaxed lamellar colonies and massive γ grains.

High degree of similarity is found in the microstructure of the blade. Specimens 6 and 8 mainly consist of short columnar grains and equiaxed (α_2+γ) grains. A large number of massive precipitated γ phases are found, as shown in Figs. 7(a) and (c). At the center of the blade body [Fig. 7(b)], columnar grains are hardly found, and the volume fraction of equiaxed (α_2+γ) grains is higher than that of the specimens at blade tip. SEM observations reveal that at blade body positions, no significant difference in microstructure is found between the edge and center of Specimens 6, 7, and 8. Specimens 6 and 8 exhibit a high volume fraction of precipitated γ phase, as shown in Figs. 8(a), (b), (e), and (f). However, Specimen 7 exhibits significantly fewer γ phase precipitates and a notably larger average grain size, as shown in Figs. 8(c) and (d).

In conclusion, for TiAl alloys, the formation of (α_2+γ) columnar or equiaxed grains is mainly influenced by two main factors: the direction of heat dissipation and the cooling rate. During the solidification process, if a certain position is dominated by unidirectional heat flow and a low cooling rate, the grains tend to grow directionally along the opposite direction of heat flow, resulting in columnar grains. However, under the circumstances of isotropic heat dissipation and high cooling rate, the grains tend to nucleate and grow uniformly in various directions, therefore forming equiaxed grains.

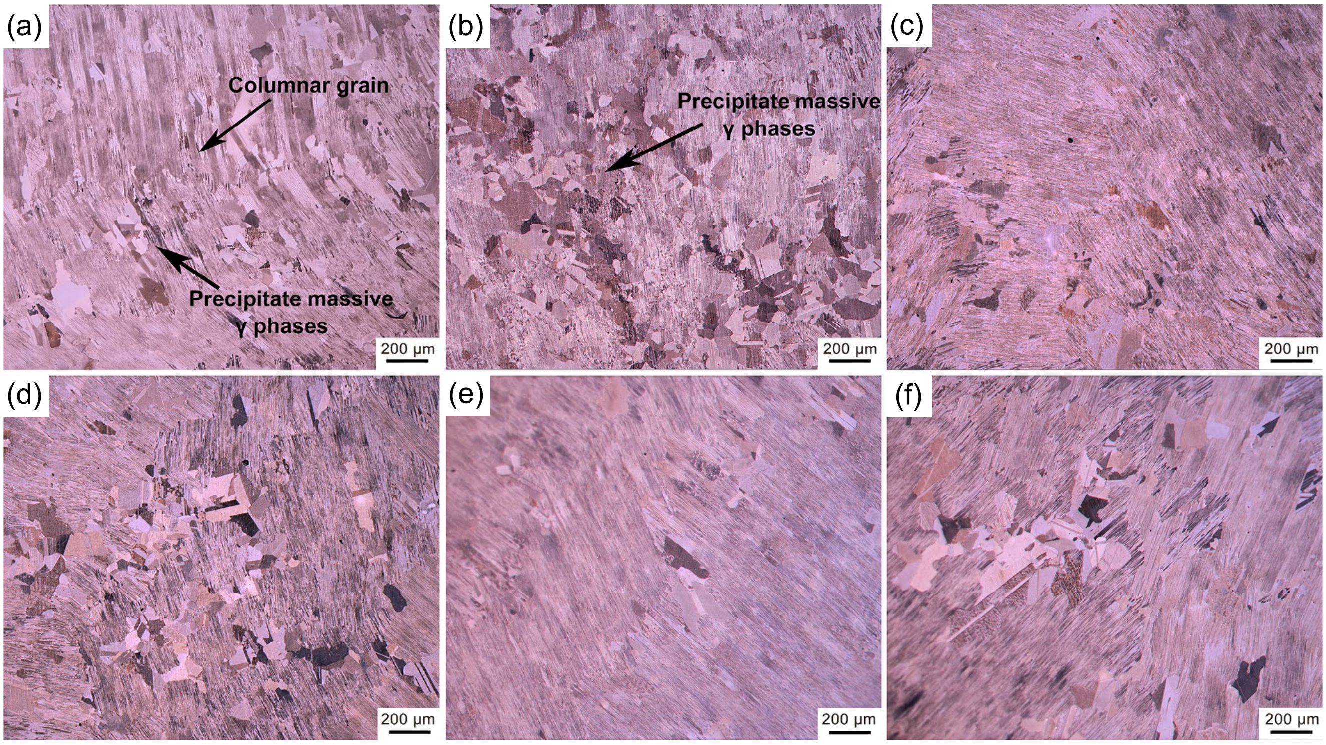

Fig. 5: Microstructure of metallographic specimens at turbine hub: (a) Specimen 1, edge; (b) Specimen 1, center; (c) Specimen 3, edge; (d) Specimen 3, center; (e) Specimen 5, edge; (f) Specimen 5, center

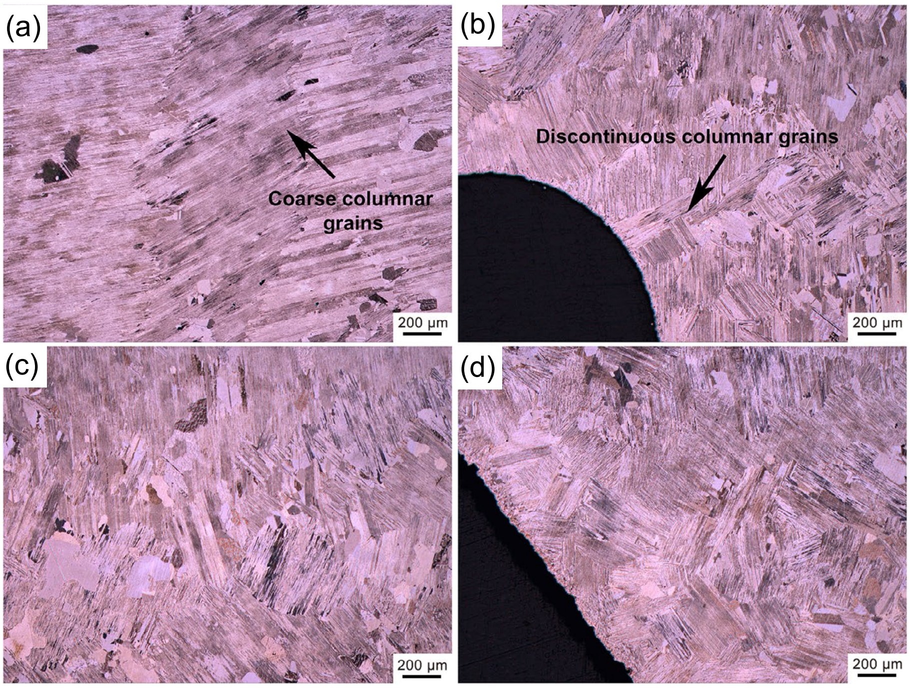

Fig. 6: Microstructure of metallographic specimens at blade root: (a) Specimen 2 adjacent to turbine hub; (b) Specimen 2 adjacent to blade body; (c) Specimen 4 adjacent to turbine hub; (d) Specimen 4 adjacent to blade body

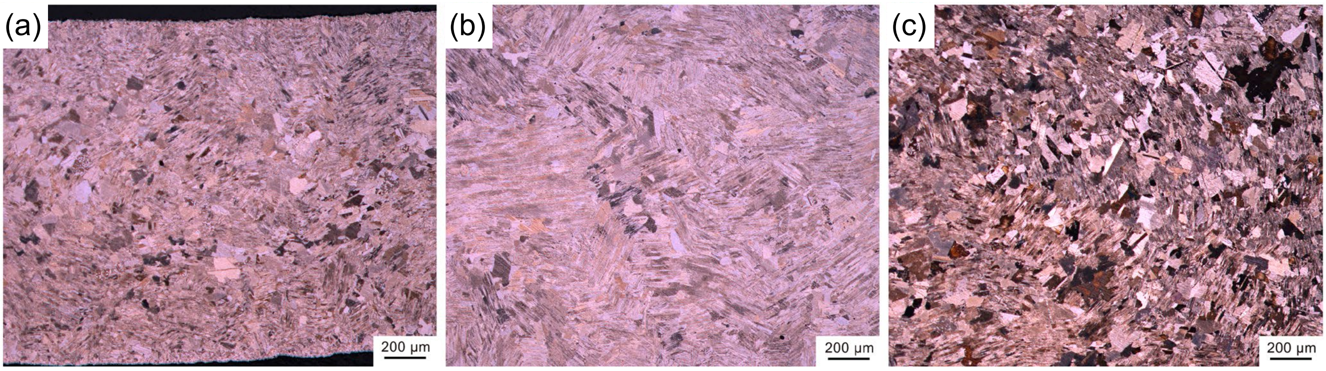

Fig. 7: Microstructure of metallographic specimens at blade body: (a) Specimen 6; (b) Specimen 7; (c) Specimen 8

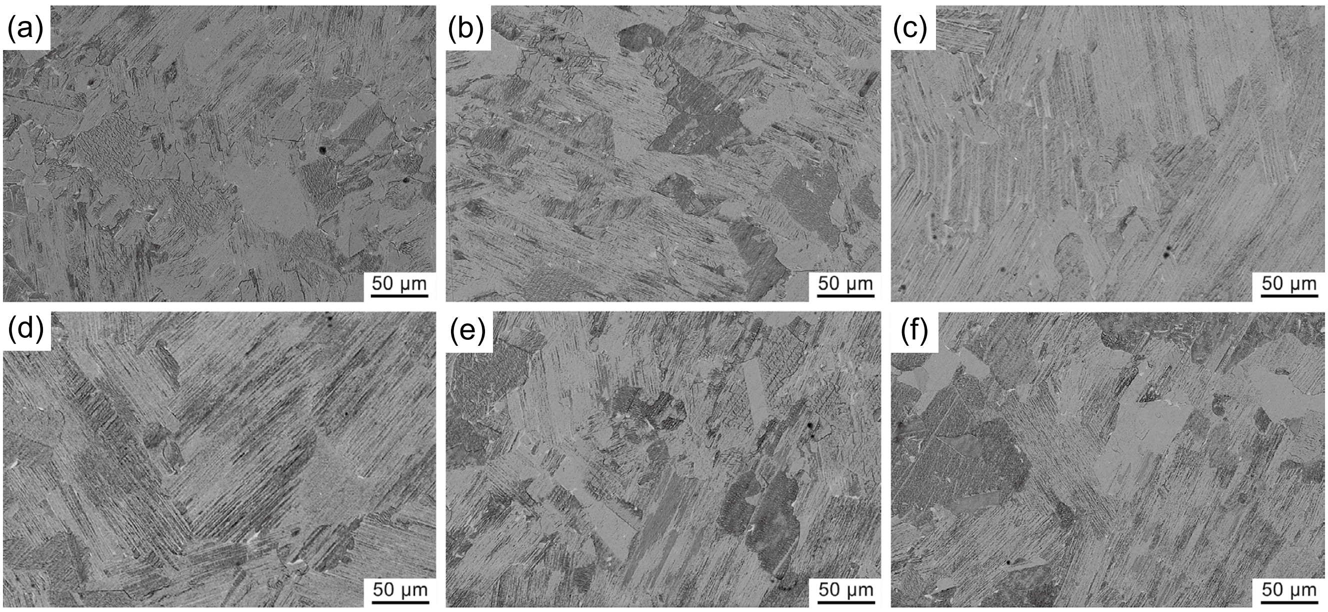

Fig. 8: Edge and center microstructure of metallographic specimens at blade body: (a) Specimen 6, edge; (b) Specimen 6, center; (c) Specimen 7, edge; (d) Specimen 7, center; (e) Specimen 8, edge; (f) Specimen 8, center

Specifically, for the case of turbine, the turbine hub is relatively thick, and during solidification, the unidirectional heat flow is from the center to the surface. Additionally, the thick structure leads to slow heat transfer, low cooling rate, and low degree of undercooling at the solidification front, meeting the conditions for the formation of columnar grains. For the blades, the heat dissipation is isotropic, and both the blade structure and the mold are relatively thin, which allows the heat to dissipate uniformly in all directions and results in a high cooling rate. Therefore, blades show a tendency to exhibit equiaxed grains.

3.2 Phase constitution in different regions of turbine

To describe the solidification path of the alloy, with reference to the Ti-Al binary phase diagram[19], the Al-equivalent method can be used to convert the influence of other alloying elements on the solidification path into an equivalent Al content[20]. Han et al.[21] proposed that the Ti/Al atomic ratio is an important parameter affecting the microstructure. In order to investigate the relationship between the Ti/Al atomic ratio and the microstructure, EDS analysis was carried out to acquire the average Ti/Al atomic ratios at the edge and center of each specimen, as shown in Fig. 9. During the solidification process, considering that the partition coefficient of Al is less than 1, Al is preferentially rejected from the solidifying dendrites into the liquid phase. Consequently, the dendrites are enriched in high-melting-point elements such as Ti or Nb, while the liquid phase concentrated with Al[22, 23]. Since the liquid phase exists longer in the interior of the casting than at the surface during the cooling period, for all specimens at the turbine hub and the blade root regions, Ti/Al atomic ratios at the center of specimens are generally lower than those at the edge.

The volume fractions of (α_2+γ) lamellar colonies and γ phases in each specimen were counted, as shown in Fig. 10. The primary factor promoting the precipitation of γ phases is the shift of the solidification path toward Al in the phase diagram. The lower the average Ti/Al atomic ratio of the sample, the more likely it is to exhibit a greater amount of γ phase in the microstructure. For Specimen 1, which has the lowest Ti/Al atomic ratio at the edge and the second lowest Ti/Al atomic ratio at the center, possesses the highest γ phase fraction of 14.028%. While, Specimens 2–5 exhibit similar volume fractions of γ phase from

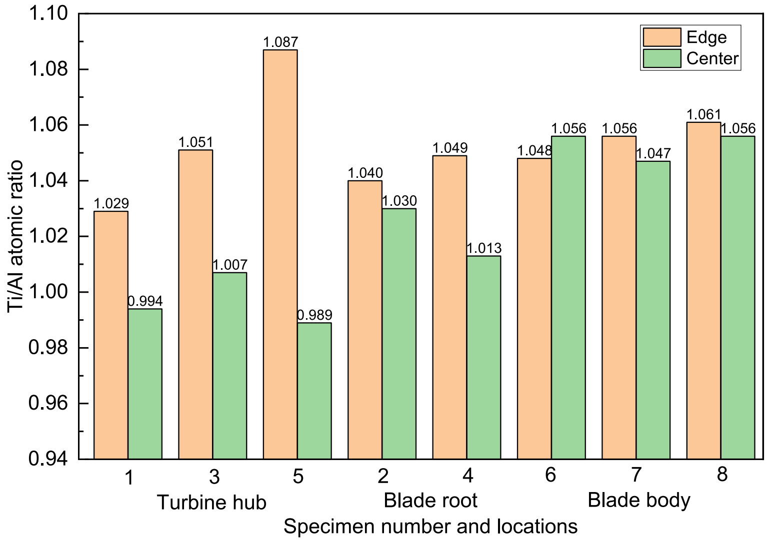

Fig. 9: Ti/Al atomic ratio at the edge and center of Specimens 1–8

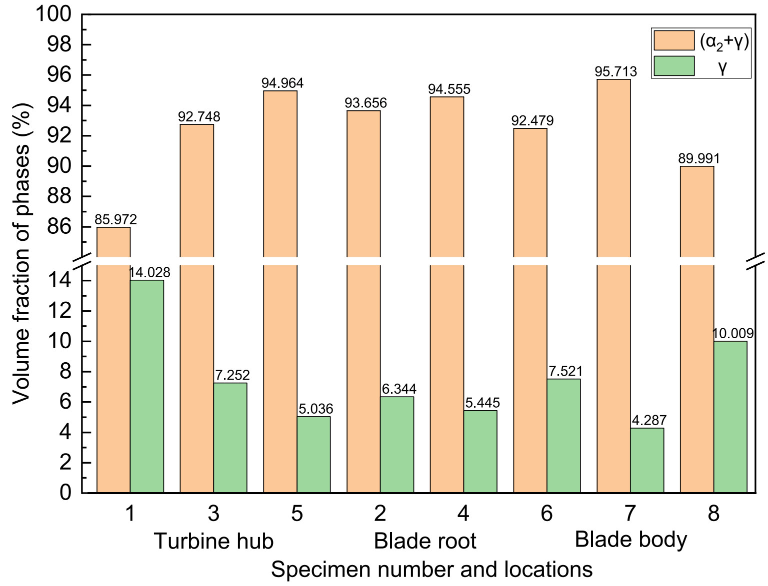

Fig. 10: Volume fractions of (α_2+γ) lamellar colonies and massive γ phases of Specimens 1–8

5.036% to 7.252%. At the blade body regions, despite the relatively high Ti/Al atomic ratio, the rightward shift of the solidification path due to non-equilibrium solidification under rapid casting cooling cannot be neglected. This shift consequently inhibits the occurrence of peritectic solidification. Particularly, Specimens 6 and 8 exhibit relatively high γ phase fractions of 7.521% and 10.009%, respectively. This is because the specimens are located at the edge of the casting, where the higher cooling rate promoted the precipitation of γ phase. Specimen 7 features a relatively low cooling rate and a lower γ phase fraction.

3.3 Hardness

Average Vickers microhardness (HV) and Rockwell hardness (HRC) of different specimens are shown in Fig. 11. The average HV of each specimen changes between 230.00 and 295.05. Significant correlation is found between the specimen sampling positions and the average HV values. The average HV of the hub regions (Specimens 1, 3, and 5) ranges from 230.00 to 246.21, with an overall mean of 238.40. In

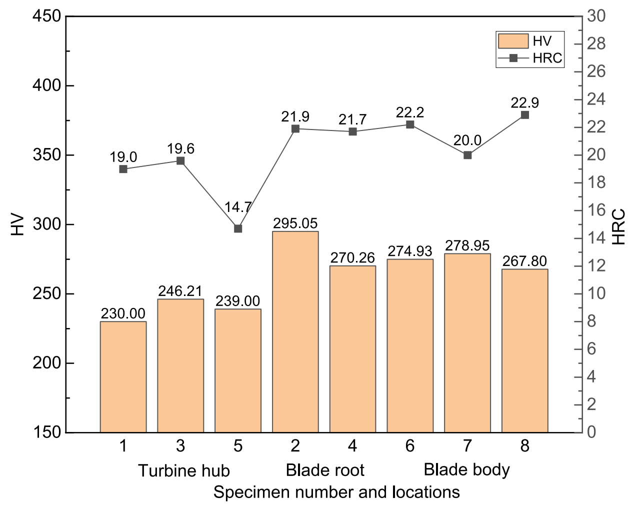

Fig. 11: Average Vickers hardness (HV) and Rockwell hardness (HRC) in different regions

contrast, the blade body (Specimens 6, 7, and 8) exhibits a narrower hardness range of 267.80 HV to 274.93 HV, with an average of 273.89 HV. Specimen 4, located at the blade root, has an average HV of 270.26, which is similar to that of the blade body specimens. The highest average HV of 295.05 is observed in Specimen 2, located at the leading-edge root. Consequently, the overall average HV at the blade root is 282.66.

The average Rockwell hardness values for the turbine hub, blade root, and blade body are 17.8, 21.8, and 21.7, respectively. The results of the macro HRC test at the same regions corroborate the phenomenon of microhardness: the turbine hub exhibits relatively low hardness, while the blade root and blade body show similarly higher hardness values. This is mainly attributed to the blade root, which is a transition zone between the blade body and the turbine hub. During solidification, the blady root experiences a relatively high cooling rate along with a partially unidirectional heat flow, resulting in a mixed microstructure of short columnar grains and equiaxed grains, as shown in Fig. 6. The short columnar grains provide great strength along the direction of main stress, while the equiaxed grains contribute to isotropic strength and higher toughness.

The stress concentration regions during operation are located at the blade roots, while blade roots exhibit higher strength than the turbine hub and the blade body, proving the benefit of this gravity casting process for the performance of turbines.

4 Conclusions

This study investigated the microstructural characteristics of gravity investment casting TiAl turbine, indicating the relationship between geometric structure, cooling rate, microstructure and hardness. The main conclusions are summarized as follows:

(1) In gravity casting, the cooling rate at the bottom of the turbine hub is lower than that at the top. Moreover, the cooling rates of the turbine hub are lower than those of the blade body, and the blade tip exhibits the highest cooling rate. The average grain size exhibits a significant negative correlation with the cooling rate.

(2) Because of the unidirectional heat flow and low cooling rate, the turbine hub and blade root are dominated by coarse and continuous columnar grains. In contrast, isotropic heat dissipation and high cooling rate result in discontinuous columnar grains and equiaxed grains.

(3) The volume fraction of massive γ phase is influenced by both the Ti/Al atomic ratio and the cooling rate. Lower Ti/Al atomic ratio and higher cooling rate promote the solidification path to shift to the Al side of the Ti-Al phase diagram, therefore promoting the precipitation of γ phase. The highest γ phase volume fractions are observed at the top region of the turbine hub and the lower blade tip, reaching 14.028% and 10.009%, respectively.

(4) The average Vickers hardness and Rockwell hardness at the blade root are slightly higher than those at the blade body, and significantly higher than those at the hub, proving the method of gravity investment casting in optimizing the microstructure of the blade root and the overall mechanical properties of the turbine.

Conflict of interest

The authors declare that they have no conflict of interest.

References

[1] Genc O, Unal R. Development of gamma titanium aluminide (γ-TiAl) alloys: A review. Journal of Alloys and Compounds, 2022, 929: 167262.

[2] Zheng G M, Tang B, Zhao S K, et al. Evading the strength-ductility trade-off at room temperature and achieving ultra high plasticity at 800 °C in a TiAl alloy. Acta Materialia, 2022, 225: 117585.

[3] Musi M, Graf G, Clemens H, et al. Alloying elements in intermetallic γ-TiAl based alloys – A review on their influence on phase equilibria and phase transformations. Advanced Engineering Materials, 2023, 26(4). Http://dor.org/10.1002/adem.202300610.

[4] Xu X, Ding H, Huang H, et al. Twin and twin intersection phenomena in a creep deformed microalloyed directionally solidified high Nb containing TiAl alloy. Journal of Materials Science & Technology, 2022, 127: 115–123.

[5] Liu J H, Pan Y, Sun J Z, et al. Preparation of complex thin-walled TiAl alloy swirlers by powder injection molding. Journal of materials engineering. Journal of Materials Engineering, 2024, 52(12): 67–79.

[6] Zhu C L, Liu Y, Zhang J, et al. Research progress of titanium aluminide turbocharger turbine. Journal of Netshape Forming Engineering, 2022, 14(1): 62–70.

[7] Tetsui T, Ono S. Endurance and composition and microstructure effects on endurance of TiAl used in turbochargers. Intermetallics, 1999, 7(6): 689–697.

[8] Tetsui T. Development of a second generation TiAl turbocharger. Materials Science Forum, 2007, 561–565: 379–382.

[9] Zhang F Q, Ding X F, Nan H, et al. Microstructures and phase transformation in directionally solidified TiAl-Nb alloys. China Foundry, 2020, 17(6): 402–408.

[10] Tetsui T. Development of a TiAl turbocharger for passenger vehicles. Materials Science and Engineering: A, 2002, 329: 582–588.

[11] Zhu C L, Li S, Zhang J, et al. Evaluation of endurance for turbocharger wheel of TiAl based alloy. Rare Metal Materials and Engineering, 2020, 49(3): 980–984.

[12] Zhu C L, Li S, Zhang J. Microstructure design for reliability of turbocharger blade of cast TiAl based alloy. Journal of Materials Engineering, 2017, 45(6): 36–42. (In Chinese)
[13] Zhu C L, Li H Z, Luo C, et al. Influence of hot isostatic pressing treatment on stress rupture behaviour of a cast Ti-47.5Al-2.5V-1.0Cr alloy. Transaction of Materials and Heat Treatment, 2014, 35(3): 79–85.
[14] Sung S Y, Kim Y J. Modeling of titanium aluminides turbo-charger casting. Intermetallics, 2007, 15(4): 468–474.
[15] Hu H T, Zuo J B, Huang D, et al. Effects of different centrifugal casting methods on TiAl alloy turbocharger forming. Special Casting & Nonferrous Alloys, 2022, 42(7): 797–804. (In Chinese)
[16] Zhao J, Zhang Z Y, Liu S B, et al. Elimination of misrun and gas hole defects of investment casting TiAl alloy turbocharger based on numerical simulation and experimental study. China Foundry, 2020, 17(1): 29–34.
[17] Zhu X, Zhu C, Lin B, et al. Research on optimization design of cast process for TiAl case casting. Metals, 2022, 12(11): 1954. https://doi.org/10.3390/met12111954.
[18] Du S G, Wang S L, Gao M. Compression damage and tensile fracture behavior of TiAl alloy turbine. Rare Metal Materials and Engineering, 2023, 52(9): 3332–3337.
[19] Schuster J C, Palm M. Reassessment of the binary aluminum-titanium phase diagram. Journal of Phase Equilibria and Diffusion, 2006, 27(3): 255–277.
[20] Ding X F, Liu H, Zhang F Q, et al. Microstructure characteristics of the directionally solidified TiAl-Nb alloys with different solidification modes. Materials Today Communications, 2022, 32: 103770.
[21] Han J T, Jiang M Z, Zhang M C, et al. Effects of Ti/Al ratio on microstructure and tensile strength of cast TiAl alloys. Special Casting & Nonferrous Alloys, 2008(6): 475–477. (In Chinese)
[22] Hu H T, Zhang X W, Zhu C L, et al. Solidification segregation characteristics of cast TiAl alloy. Foundry, 2019, 68(7): 740–745. (In Chinese)
[23] Hu D, Botten R R. Phase transformations in some TiAl-based alloys. Intermetallics, 2002, 10(7): 701–715.